Tutorial: Experimental Nonlinear Dynamical Circuit Analysis of a Ferromagnetic Inductor

Suhas Kumar and R. Stanley Williams

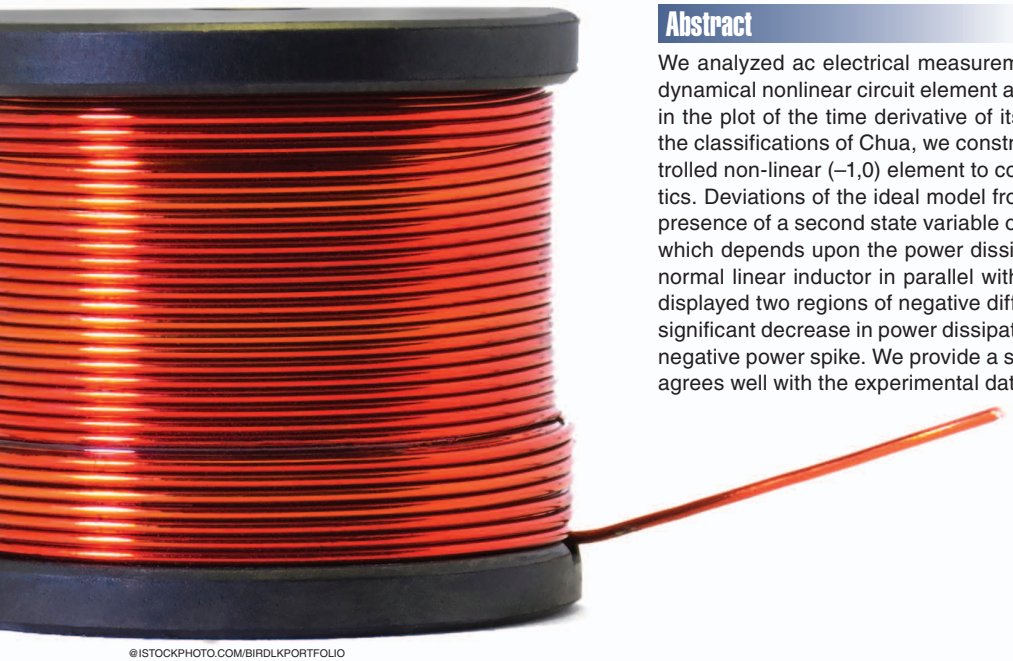

Abstract

We analyzed ac electrical measurements of a ferromagnetic inductor as a dynamical nonlinear circuit element and observed a pinched hysteresis loop in the plot of the time derivative of its current *di/dt* versus voltage *v*. Using the classifications of Chua, we constructed a model of an ideal voltage-controlled non-linear (–1,0) element to compare with the measured characteristics. Deviations of the ideal model from the experimental data indicated the presence of a second state variable or parameter, identified as temperature, which depends upon the power dissipated in the inductor. After installing a normal linear inductor in parallel with the ferromagnetic inductor, the latter displayed two regions of negative differential inductance accompanied by a significant decrease in power dissipation, while the former displayed a sharp negative power spike. We provide a simple extension of the ideal model that agrees well with the experimental data.

Chua has created a systematic framework for mathematically modeling electronic circuit elements that he has termed a periodic table. [1] Within an electronic circuit, a designer primarily cares about the currents $i(t)$ passing through devices and voltages $v(t)$ across them, which are properties that can be measured experimentally versus time. Given these basic measurements, it is then possible to differentiate or integrate the two signals, where $\alpha \geq 0$ refers to the α^{th} derivative while $\alpha < 0$ refers to the α^{th} integral of voltage with respect to time, and similarly for β with reference to current. [1] The simplest model for an ideal circuit element is

Digital Object Identifier 10.1109/MCAS.2018.2821758
Date of publication: 21 May 2018

a mathematical formula that directly connects two characteristics (α, β); for a memory element, this relationship will be represented by a nonlinear function. The usual passive resistor, capacitor and inductor are identified as (nearly) linear (0, 0), (0, –1) and (–1, 0) elements, respectively, with the memristor forming the non-linear (–1, –1) element. [2] However, real electronic devices are usually more complex than these ideal mathematical models, so Chua has defined a set of mathematical relations of increasing complexity to accommodate a broader set of observable behaviors. [1] In addition, any real device may contain characteristics of two or more model (α, β) elements—the physical device is usually called by the name of the dominant model that explains its behavior, but that can change with different inputs (e.g. voltage amplitudes or frequencies) or operating environments (e.g. temperature). The recent identification of many previously unclassified electronic devices as memristors has opened up entire new areas of research, modeling and applications. [3]–[6] Here we examine a ferromagnetic inductor (FML) in order to see what new insights might be gained from a nonlinear circuit analysis of this familiar element.

We constructed the FML using a nanocrystalline ferromagnetic toroidal core of composition $Fe_{73.5}Si_{13.5}B_9Nb_3Cu_1$, described in detail elsewhere [7]–[10], and a wire winding of known resistance. In our first measurements, we applied a sinusoidal voltage across the FML and a 30 Ω series resistor (R_S), as shown in Fig. 1a, and measured the voltage drop across R_S to determine the current $i_{FM}(t)$ and simultaneously the FML voltage $v_{FM}(t)$ (corrected for the voltage drop due to the winding) as shown in Fig. 1b. We used a sinusoidal driving voltage in order to eliminate transients in the ac signals, and we averaged over 49 cycles of steady-state operation in order to improve the signal to noise ratio in the data. In this analysis, we followed Chua and defined the flux in the FML as $\phi_{FM} = \int v_{FM}(t)dt$, [1] which was computed numerically from the experimental data and is displayed in Fig. 1b, along with several other functions derived from the measured data that will be used below.

A plot of the experimentally derived ϕ_{FM} against i_{FM} (Fig. 2a, labeled 'Expt.') shows the familiar FML hysteresis curve with relatively abrupt switching characteristics. The area contained within the hysteresis loop corresponds to the irreversible or instantaneous work used to switch the magnetization in the ferromagnetic toroid twice. We also plotted di_{FM}/dt against v_{FM} (Fig. 2b), which showed a pinched hysteresis loop, a feature familiar from i-v plots of memristors, [4], [11] that has not been shown in previous analyses of FMLs. Further, we produced a phase portrait (also known as a dynamical

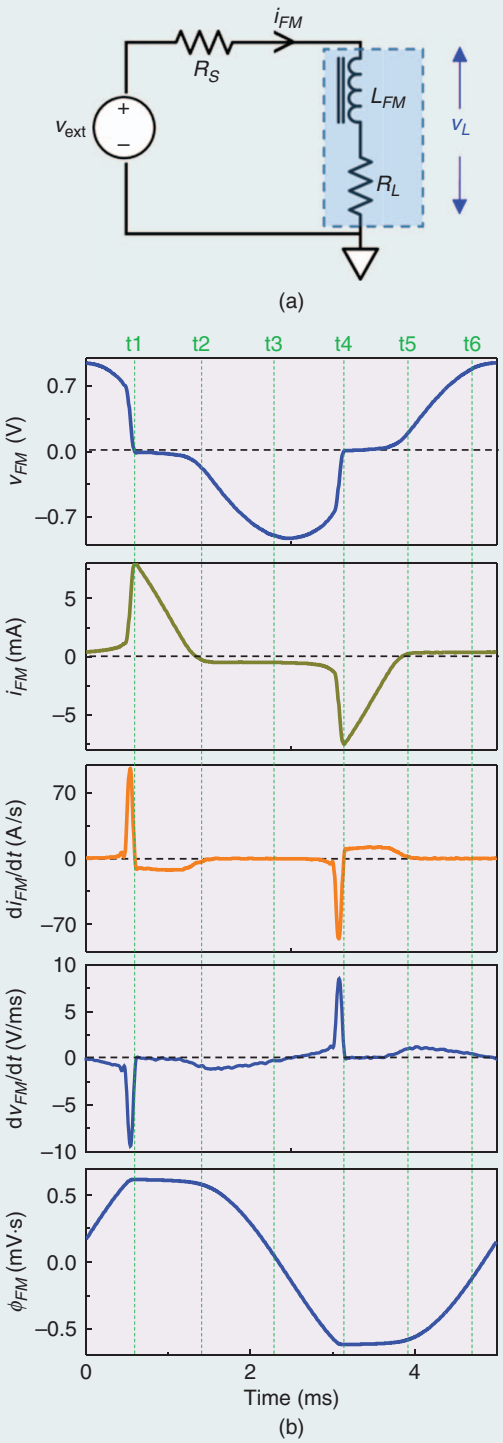

Figure 1. Ferromagnetic Inductor (FML) electrical measurements. (a) The circuit used. Dashed rectangle refers to the FML, while R_L is its winding resistance. (b) Plots of various measured and calculated functions from the circuit shown in (a). All plots are over one complete period of a 200 Hz sinusoidal v_{ext}, averaged over 49 successive periods after steady-state operation for better signal-to-noise ratio.

Suhas Kumar and R. Stanley Williams are with the Hewlett Packard Labs, 1501 Page Mill Rd, Palo Alto, CA 94304, USA.

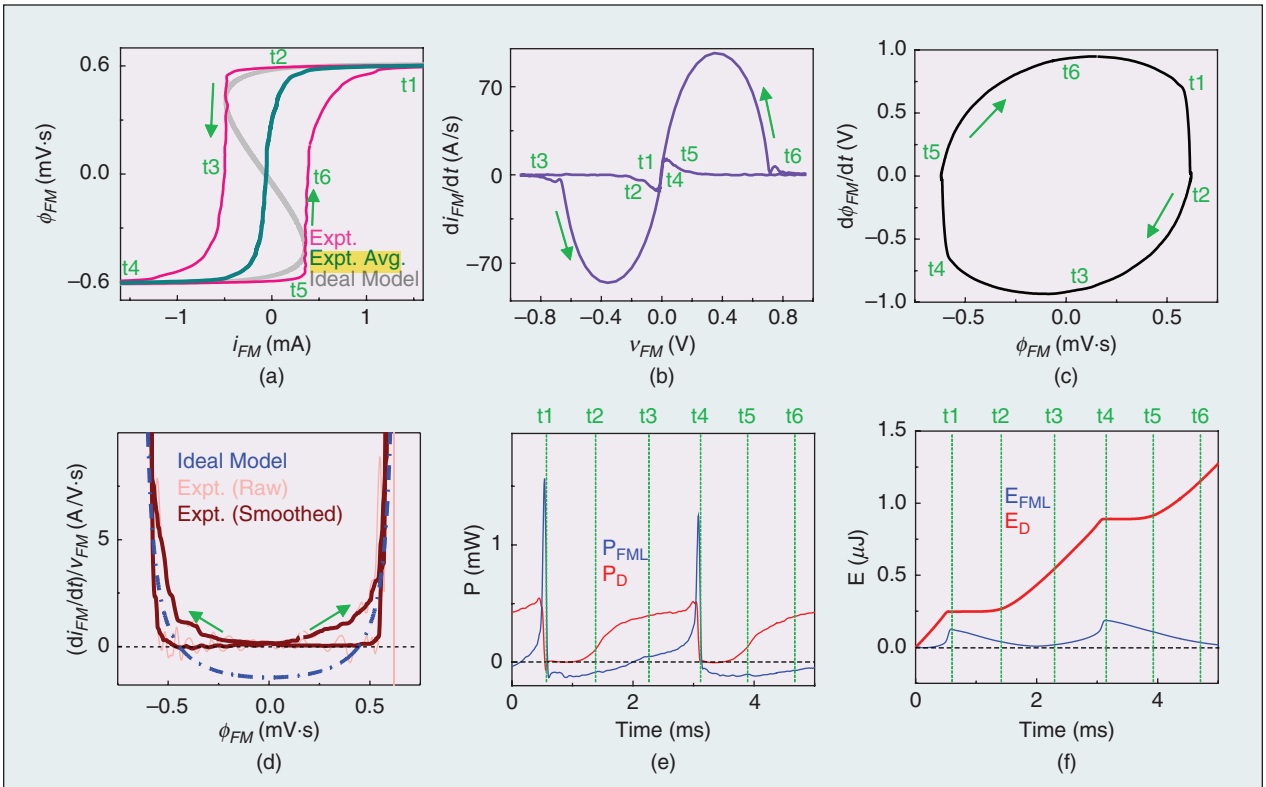

Figure 2. FML characterization. (a) Plot of ϕ_{FM} against i_{FM} from experimental data (red curves 'Expt.'), from the calculation of a restoring function (green curve 'Expt. Avg.'), and the comparison to an ideal non-linear (–1,0) element (gray curve 'Ideal model'). 't1'–'t6' are temporal markers. (b) Plot of di_{FM}/dt against v_{FM}, exhibiting a pinched hysteresis loop. (c) Plot of $d\phi_{FM}/dt$ against ϕ_{FM}, the phase portrait. (d) Plot of $(di_{FM}/dt)/v_{FM}$ (or $\mathcal{L}_{FM}^{-1}$) against ϕ_{FM} for the experimentally derived data (raw and smoothed). Ideal model corresponds to Equation 4. (e)-(f) Plots of powers and energies vs. time, for the restoring function, or reversible stored flux ('FML') and the dissipative component ('D') that causes heating during the ferromagnetic switching.

route map) [12] of the system by plotting $d\phi_{FM}/dt$ vs. ϕ_{FM} (Fig. 2c), wherein the zero-crossings $(d\phi_{FM}/dt)=0$ represent regions of slowest state speed for the driven system near the time markers t2 and t5, while the values of ϕ_{FM} at the maximum and the minimum of $d\phi_{FM}/dt$ are the regions of maximum state speed near t3 and t6, where the trajectory of the system sweeps rapidly past $\phi_{FM}=0$.

How can we construct a compact dynamical nonlinear model for the FML? [13], [14] One approach is to consider the FML to be a black box, [15] and to use an 'unfolding' process [16] to determine functions characterizing the static and dynamical properties of the FML as polynomials in one or more variables. This method can yield a very accurate mathematical representation of the electrical characteristics of the FML if the polynomials have a large number of terms, but does not provide much physical insight into the functioning of the FML. We desired the simplest model that provides intuition at the possible expense of accuracy, which meant that instead of following a well-defined procedure we used a trial and error approach using our data to determine an approximate functional form. We therefore created a first approximation with the equations defining a voltage-controlled (–1,0) element:

$$\frac{di}{dt}=\mathcal{L}_{FM}^{-1}(\phi_{FM})v, \tag{1}$$

$$\frac{d\phi_{FM}}{dt}=v \tag{2}$$

where $\mathcal{L}_{FM}^{-1}=(di/d\phi_{FM})$ is the inverse differential (or incremental) inductance, which is not the same as the inverse integral inductance $L_{FM}^{-1}=(i/\phi_{FM})$ for a nonlinear system. We used the inverse $\mathcal{L}_{FM}^{-1}$ rather than $\mathcal{L}_{FM}$ because the latter diverges, is undefined for certain values of ϕ_{FM} and is therefore an inappropriate mathematical description of the element. Equation 2 is Chua's definition of flux and is also the dynamical equation for the voltage-controlled ideal non-linear (–1,0) element. Together the equations imply that a plot of di/dt vs. v should be a pinched hysteresis loop, shown by the experimental data (Fig. 2b) and confirming that the device is indeed a non-linear (–1,0) element. [1], [17] The name 'meminductor' is appropriate for a hypothetical

non-linear (–2,–1) element, [1], [17] which has been incorrectly identified as an FML. [18] The ferroelectric capacitor, which can be classified as a non-linear (0,–1) element, is symmetric with respect to the FML in the periodic table of circuit elements [1].

The next step in creating the model is to determine a functional form for $\mathcal{L}_{FM}^{-1}(\phi_{FM})$. One approach is to utilize a polynomial formula $\mathcal{L}_{FM}^{-1}(\phi_{FM}) = a_0 + a_2\phi_{FM}^2 + a_4\phi_{FM}^4 + \ \ldots$ A problem with this approach is the difficulty in modeling the rapid saturation of ϕ_{FM} with respect to i in Fig. 2a. The initial model we have chosen for the inverse differential inductance of the ideal non-linear (–1,0) element is the following:

$$\mathcal{L}_{FM}^{-1}(\phi_{FM}) = \gamma\left(\frac{\phi_s}{\phi_s^2 - \phi_{FM}^2} + \xi\right), \tag{3}$$

where $\phi_s = 0.63$ mVs is the saturation flux, and $\xi = -3$ and $\gamma = 10^{-3}$ are constants. Alternately, we can write the expression for the inverse integral inductance:

$$L_{FM}^{-1}(\phi_{FM}) = \gamma\left[\frac{atanh\left(\frac{\phi_{FM}}{\phi_s}\right)}{\phi_{FM}} + \xi\right] \tag{4}$$

A plot of ϕ vs. i obtained by parametrically sweeping ϕ in Equation 4 and using $i = \phi_{FM}L_{FM}^{-1}$ produces a single-valued function of ϕ (Fig. 2a, gray curve labeled 'Ideal Model') that clearly shows two regions of negative differential inductance (NDL) underlying the experimentally observed hysteretic behavior. We note that the presence of a negative differential behavior is often a signature of local activity, or the ability of a system to store and release energy during its operation. [12] Hence this ideal model represents a locally active non-linear (–1,0) element. A plot of $\mathcal{L}_{FM}^{-1}(\phi_{FM}) = (1/v)(di/dt)$ vs. ϕ_{FM} for both the experimentally measured data and the ideal model (Fig. 2d) shows first that there are two branches in the experimental data instead of the single curve of the ideal model, and second that the NDL predicted by the model ($\mathcal{L}_{FM}^{-1}(\phi_{FM}) < 0$) is not accessed by the experimental measurements.

The fact that the plot of $\mathcal{L}_{FM}^{-1}(\phi_{FM}) = (1/v)(di/dt)$ vs. ϕ_{FM} from experimental data did not yield a single curve but rather two branches shows that the system is not ideal. There is likely a second state variable or parameter that causes $\mathcal{L}_{FM}^{-1}$ to vary, such as the temperature of the device. Newton's law of cooling, [19], [20]

$$\frac{dT}{dt} = \frac{P_D}{C_{th}} - \frac{T - T_{amb}}{C_{th}R_{th}}, \tag{5}$$

where T is the temperature of the inductor, T_{amb} is the ambient temperature of the surroundings, C_{th} is the heat capacity, R_{th} is the effective thermal resistance, and P_D is the dissipated power, has been utilized successfully to model temperature variations in memristors during operation. Equation 5 defines a second state variable for the system, or if the thermal time constant is much smaller than the period of the driving voltage, the steady state approximation $(dT/dt) = 0$ can be used to define a power-dependent parameter T. The problem in evaluating Equation 5 for a FML is that $P_D \neq i_{FM}v_{FM}$; there are both reversible power in the inductor P_{FML} and power dissipated P_D in switching the magnetization of the ferromagnetic torus (and to a lesser extent inducing eddy currents). Fortunately, Chua has provided an ingenious technique to determine restoring and dissipative functions for systems with hysteresis. [21]–[23] A non-hysteretic ϕ vs. i plot that represents a nonlinear inductor that only stores and releases energy is determined by simply averaging the two branches of the hysteresis plot, as shown by the green curve labeled 'Expt. Avg.' in Fig. 2a. Using this result, we plot P_{FML} (blue curve) and $P_D = i_{FM}v_{FM} - P_{FML}$ (red curve) in Fig. 2e. We see that P_{FML} has both positive and negative values, corresponding to storing and releasing energy to the circuit, respectively, whereas P_D is always ≥ 0. In the FML, energy is stored during a narrow and sharp positive peak in P_{FML} and subsequently released back to the circuit as a negative P_{FML} gradually over time. The corresponding energies obtained by integrating the powers over time (Fig. 2f) show that the magnetization switching energy dissipated is much larger than the energy stored in the inductor in each cycle. This results in both long-term heating that leads to a significant temperature increase of the inductor before a steady state is achieved with the surroundings and also a cycle-dependent temperature oscillation, which is likely the cause of the experimental differential inductance curve in Fig. 2d breaking into two branches.

The hysteresis in the experimental FML ϕ vs. i plot meant that there was an instability that did not allow the measurement to directly access the NDL behavior, which is similar to the hysteresis observed for a voltage sweep of a current-controlled negative differential resistance (CC-NDR). In order to stabilize this behavior and directly observe CC-NDR, a series resistor is added to the circuit, wherein the voltage decrease in the CC-NDR device appears as a voltage increase across the series resistor. [19], [24] Similarly, in the case of NDL, a parallel linear inductor (LL) in the circuit can allow the NDL current decrease to appear as increased current in the LL. We therefore measured the circuit after installing a 27 mH LL in parallel to the FML (Fig. 3a) and repeated the set of measurements and calculations described above (Fig. 3b), in addition to measuring the current through the LL. In this case, the plot of ϕ_{FM} against i_{FM} (Fig. 4a) showed that the hysteresis loop had shrunk

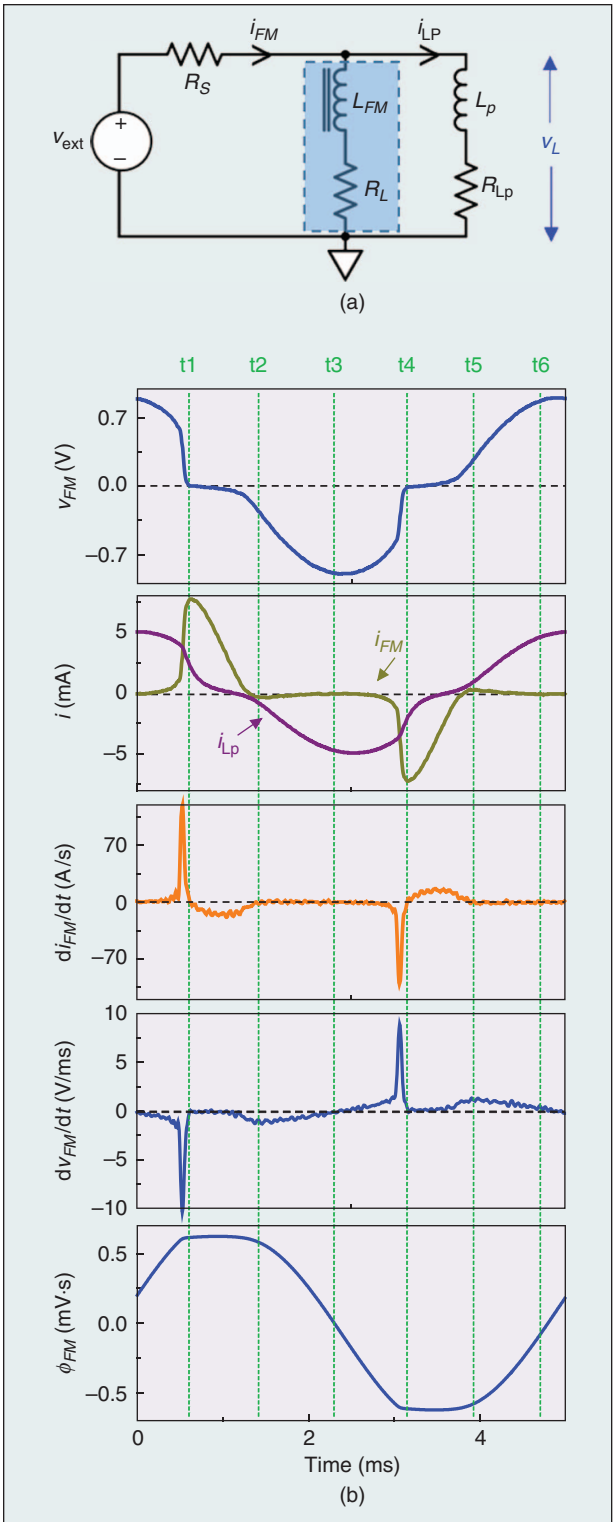

Figure 3. FML with a 27 mH parallel linear inductor (LL) electrical measurements. (a) The circuit used. Dashed rectangle refers to the FML, while R_L is its winding resistance. L_p is the parallel LL. R_{Lp} is its winding resistance. (b) Plots of various measured and calculated functions from the circuit shown in (a). All plots are over one complete period of a 200 Hz sinusoidal v_{ext}, averaged over 49 successive periods after steady-state operation for better signal-to-noise.

significantly in area, essentially breaking into two lobes, and revealed NDL regions where the current decreased as the flux increased, denoted by t5➔t6 and t2➔t3. The plots in Figs. 4b,c are similar to the corresponding plots in Figs. 2b,c (the case with no LL), confirming the identical nature of the underlying dynamics and the circuit classification of the FML despite the substantial changes in the ϕ_{FM}-i_{FM} hysteresis behavior between Figs. 2a and 4a. In the plot of $\mathcal{L}_{FM}^{-1}(\phi_{FM})$ vs. ϕ_{FM} in Fig. 4d, there is significant NDL in the experimental data that appears as two branches each with a local minimum displaced from $\phi_{FM} = 0$. The hysteresis loop did not collapse into a single-valued function of ϕ_{FM}, as with the ideal model (gray curve, Fig. 4a). The area in each lobe of the experimental data (red curves) represents an upper limit to the minimum reversible work needed to switch the magnetization of the ferromagnetic toroid, and is directly related to the double minima in the experimental $\mathcal{L}_{FM}^{-1}(\phi_{FM})$ curve, which was missing from the ideal model. We used the technique of constructing a restoring function to determine P_{FML} and P_D for the FML, which are plotted in Fig. 4e along with the measured power in the parallel LL. The power returned to the circuit (negative power) by the parallel LL was sharply peaked, large in amplitude, and available because of the large decrease in P_D of the FML. The corresponding energies, plotted in Fig. 4f reveal that the total energy per cycle dissipated by the FML was approximately a factor of three lower than the case with no LL (Fig. 2f), as was also evident in the corresponding shrinking of the area within the hysteresis loop in the ϕ vs. i plots (Figs. 2a and 4a). Thus, the steady state temperature for the FML in this circuit is significantly lower than for the stand-alone FML. However, the cycle-dependent temperature oscillations should be larger because the dissipated power in the FML is more strongly peaked, as seen by comparing Fig. 4(e) with Fig. 2(e), which has a significant influence on the electronic behavior during a voltage cycle. The high peak power returned to the circuit by the LL is useful for some applications for which amplifiers or active devices are not suitable or are otherwise unavailable.

While an accurate predictive model will require careful static and dynamic temperature measurements to correlate with the electronic behavior, it is possible to determine a heuristic temperature-dependent functional form for the inverse differential inductance that displays the minima observed in the FML experimental data, as described by Equation 6.

$$\mathcal{L}_{FM}^{-1}(\phi_{FM}, T) = \gamma\left[\frac{\phi_{FM}^2}{\phi_S^2 - \phi_{FM}^2} + \xi(T)\left(\frac{\phi_{FM}^2}{\phi_S^2}\right)\right], \qquad (6)$$

where $\xi(T)$ is a temperature-dependent parameter. Since the dynamics of the system cause significant

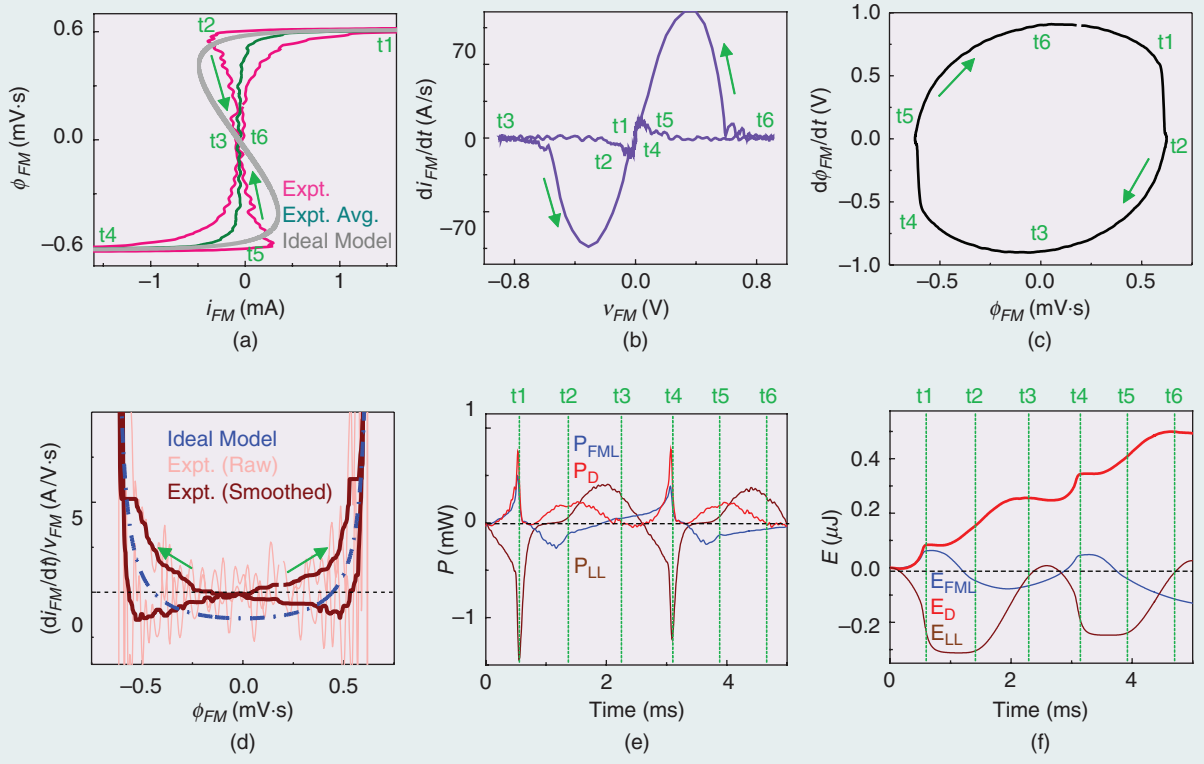

Figure 4. FML with parallel LL characterization. (a) Plot of ϕ_{FM} against i_{FM} from experimental data (red curves 'Expt.'), from calculation of the restoring function (green curve 'Expt. Avg.'), and the same model as in Fig. 2(a) (gray curve 'Ideal model'). 't1'–'t6' are temporal markers. (b) Plot of di_{FM}/dt against v_{FM}, exhibiting a pinched hysteresis loop. (c) Plot of $d\phi_{FM}/dt$ against ϕ_{FM}. (d) Plot of $(di_{FM}/dt)/v_{FM}$ (or $\mathcal{L}_{FM}^{-1}$) against ϕ_{FM} for experimental data (raw and smoothed). Ideal model corresponds to Equation 4. (e)-(f) Plots of powers and energies vs. time, for the restoring function or reversible stored flux ('FML'), the dissipative component ('D') that causes the ferromagnetic switching, and for the 27 mH parallel linear inductor ('LL'). The small but noticeable net gain in E_{FML} and loss in E_{LL} are calculation artifacts attributed to small changes in the resistances by a few Ohms, which can be time and temperature dependent.

temperature variations, it is possible to use two extreme values of $\xi(T)$ that represent dissipation and storage of energy in the FML to approximate the dynamical behavior. Using a negative value of $\xi(T) = -4.5$ that indicates minimal energy dissipation, we were able to reproduce the pronounced minima found in the two branches of the experimental plot of $\mathcal{L}_{FM}^{-1}(\phi_{FM})$ vs. ϕ_{FM} for the case with a parallel LL in the circuit, while using positive or smaller magnitude negative values of $\xi(T)$, we were able to fit to the rest of the curves (for both the circuits with and without the LL), as shown in Fig. 5. This relationship introduces

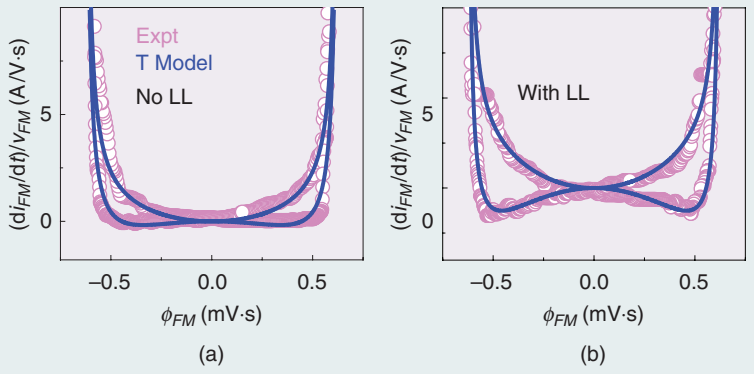

Figure 5. Flux and temperature dependent inverse differential inductance for the FML. Plots of $(di_{FM}/dt)/v_{FM}$ (or $\mathcal{L}_{FM}^{-1}$) against ϕ_{FM}. Experimental data ('Expt.', pink circles) and the generic non-linear (–1,0) element inverse differential inductance $\mathcal{L}_{FM}^{-1}(\phi_{FM}, T)$ ('T model') corresponding to Equation 6. (a) Case with no LL. Set of $\xi(T)$ used was (+1,–2) for the two component curves displayed. (b) Case with a LL. Set of $\xi(T)$ used was (+3,–4.5) for the two component curves displayed.

the temperature as a state parameter, but if the steady state approximation does not hold for Equation 5, temperature would become a state variable for the FML, which would then be classified as a generic (–1,0) nonlinear element. In contrast, a normal inductor (one that does not contain a ferromagnetic core) does not exhibit an appreciable degree of non-linearity or any form of local activity, and thereby is classified as a linear (–1,0) element.

In conclusion, by measuring only voltage and current simultaneously as a function of time, we were able to compute several interesting functions from the experimental data to help analyze the nonlinear dynamical properties of a FML. This complements the usual analysis in terms of the energy of a magnetic phase transition as the ferromagnetic system crosses an energy barrier between two stable equilibria, formalized by several Mean Field theories including the Landau model. [25], [26] We also showed that this element exhibited negative differential inductance, which is an indicator of local activity or the ability of the system to store energy and use it to amplify small changes to the input. [12] We analyzed a heuristic model based on an ideal voltage-controlled non-linear (–1,0) element that approximated the FML electronic behavior and illuminated the underlying circuit principles. We then introduced both the flux and temperature of the FML as two important state variables that are required to account for the complete dynamics of its behavior in a generic non-linear (–1,0) element model. The fact that this system has regions of negative differential inductance and thus local activity may be useful for constructing interesting oscillators and observing coupled dynamics in circuits that have not yet been explored. [19]

Acknowledgments

The authors gratefully thank Leon O. Chua for providing constructive comments on this manuscript.

Suhas Kumar is a Researcher at Hewlett Packard Labs, Palo Alto, CA, USA. He earned a Ph.D. from Stanford University in 2014. He leads a group that investigates novel physical properties of materials and devices relevant to new forms of physics-driven and bio-inspired computing. His latest work includes a practical demonstration of the idea of using chaos to accelerate solutions to computationally hard problems. His research has been featured in dozens of scientific publications, conferences, patent applications, and popular media. His contributions were recently acknowledged with the Klein Scientific Development award.

R. Stanley Williams (SM'08) received the Ph.D. degree in physical chemistry from UC Berkeley, Berkeley, CA, USA, in 1978. He is a Hewlett Packard Enterprise Senior Fellow. He has >220 US patents and >440 publications in reviewed scientific journals.

References

[1] L. O. Chua, "Nonlinear circuit foundations for nanodevices. I. The four-element torus," *Proc. IEEE*, vol. 91, pp. 1830–1859, 2003.

[2] L. Chua, "Memristor: The missing circuit element," *IEEE Trans. Circuit Theory,* vol. 18, pp. 507–519, 1971

[3] T. Prodromakis, C. Toumazou, and L. Chua, "Two centuries of memristors," *Nature Mater.*, vol. 11, pp. 478–481, 2012.

[4] D. B. Strukov, G. S. Snider, D. R. Stewart, and R. S. Williams, "The missing memristor found," *Nature*, vol. 453, pp. 80–83, 2008.

[5] J. J. Yang, M. X. Zhang, J. P. Strachan, F. Miao, M. D. Pickett, and R. D. Kelley et al., "High switching endurance in TaOx memristive devices," *Appl. Phys. Lett.*, vol. 97, pp. 232102–232102-3, 2010.

[6] M. D. Pickett, G. Medeiros-Ribeiro, and R. S. Williams, "A scalable neuristor built with Mott memristors," *Nature Mater.*, vol. 12, pp. 114–117, Dec. 16, 2012.

[7] N. O. Gonchukova and S. L. Ratushniak, "Rheological properties of amorphous alloys and their description on the base of linear viscoelastic theory," *J. Phys. Conf. Ser.*, vol. 98, p. 072001, 2008.

[8] J. Silveyra, J. Moya, V. Cremaschi, D. Janičkovič, and P. Švec, "Structure and soft magnetic properties of FINEMET type alloys: Fe73.5Si13.5Nb3 – x Mo x B9Cu1 (x = 1.5, 2)," *Hyperfine Interact.*, vol. 195, pp. 173–177, 2010.

[9] N. V. Ershov, A. P. Potapov, N. M. Kleinerman, N. K. Yurchenko, V. V. Serikov, V. A. Lukshina et al., "Structure of nanocrystals in finemets with different silicon content and stress-induced magnetic anisotropy," in *Nanocrystals*. INTECH Open Access Publisher, 2011.

[10] J. Zhu, N. Clavaguera, M. T. Clavaguera-Mora, and W. S. Howells, "Neutron diffraction analysis on FINEMET alloys," *J. Appl. Phys.*, vol. 84, pp. 6565–6569, 1998.

[11] L. Chua, "Everything you wish to know about memristors but are afraid to ask," *Radioengineering*, vol. 24, p. 319, 2015.

[12] K. Mainzer and L. Chua, *Local Activity Principle*. London: Imperial College Press, 2013.

[13] L. Chua, "Device modelling via basic nonlinear circuit elements," *IEEE Trans. Circuit Syst.*, vol. 27, pp. 1014–1444, 1980.

[14] L. Chua, "Nonlinear circuits," *IEEE Trans. Circuits Syst.*, vol. 31, pp. 69–87, 1984.

[15] L. Chua, "Modeling of three terminal devices: A black box approach," *IEEE Trans. Circuit Theory*, vol. 19, pp. 555–562, 1972.

[16] L. O. Chua, "Global unfolding of Chua's circuit," *IEICE Trans. Fundam. Electron. Commun. Comput. Sci.*, vol. 76, pp. 704–734, 1993.

[17] L. Chua, "Resistance switching memories are memristors," *Appl. Phys. A*, vol. 102, pp. 765–783, 2011.

[18] Y. V. Pershin and M. Di Ventra, "Memory effects in complex materials and nanoscale systems," *Adv. Phys.*, vol. 60, pp. 145–227, 2011.

[19] S. Kumar, J. P. Strachan, and R. S. Williams, "Chaotic dynamics in nanoscale NbO_2 Mott memristors for analogue Computing," *Nature*, vol. 548, pp. 318–321, 2017.

[20] A. S. Alexandrov, A. M. Bratkovsky, B. Bridle, S. E. Savel'ev, D. B. Strukov, and R. S. Williams, "Current-controlled negative differential resistance due to Joule heating in TiO2," *Appl. Phys. Lett.*, vol. 99, p. 202104, 2011.

[21] L. Chua and S. Bass, "A generalized hysteresis model," *IEEE Trans. Circuit Theory*, vol. 19, pp. 36–48, 1972.

[22] L. O. Chua and K. A. Stromsmoe, "Mathematical model for dynamic hysteresis loops," *Int. J. Eng. Sci.*, vol. 9, pp. 435–450, 1971.

[23] L. Chua and K. Stromsmoe, "Lumped-circuit models for nonlinear inductors exhibiting hysteresis loops," *IEEE Trans. Circuit Theory*, vol. 17, pp. 564–574, 1970.

[24] A. Ascoli, S. Slesazeck, H. Mahne, R. Tetzlaff, and T. Mikolajick, "Nonlinear dynamics of a locally-active memristor," *IEEE Trans. Circuits Syst. I,* vol. 62, pp. 1165–1174, 2015.

[25] L. D. Landau and E. Lifshitz, "On the theory of the dispersion of magnetic permeability in ferromagnetic bodies," *Phys. Z. Sowjetunion*, vol. 8, pp. 101–114, 1935.

[26] J.-C. Tolédano and P. Tolédano, *The Landau Theory of Phase Transitions: Application to Structural, Incommensurate, Magnetic, and Liquid Crystal Systems,* vol. 14, World Scientific, 1987.